ENCIT 2018

ABCM Associação Brasileira de Engenharia e Ciências Mecânicas

17th Brazilian Congress of Thermal Sciences and Engineering
November 25th-28th, 2018, Águas de Lindóia, SP, Brazil

ENCIT-2018-0734
PATTERNS FORMED ON BI-DISPERSED SOLID-LIQUID FLUIDIZED BEDS IN NARROW TUBES

Fernando David Cúñez Benalcázar
Erick de Moraes Franklin
University of Campinas, School of Mechanical Engineering, Rua Mendeleyev, 200, Campinas, 13083-860, Brazil
fernandodcb@fem.unicamp.br, franklin@fem.unicamp.br

Abstract. *In this paper, the patterns formed on bi-dispersed solid-liquid fluidized beds were experimentally investigated. The fluidized beds are formed in a 25.4 mm-ID tube and consisted of alumina beads with 6mm diameter and aluminum beads with 4.762mm diameter, with a specific gravity of 3.69 and 2.76, respectively; therefore, the ratio between the spheres and the tube is between 4.23 to 5.33. The experiments were developed with two water flow rates corresponding to mean cross-sectional velocities of $\overline{U}$ = 0.137 and 0.164m/s, and six different arrangements of beds were used. With these conditions, it was possible to observe the formation of transverse waves, in the form of granular plugs (for alumina beads), and in the form of granular clusters (for aluminum beads), that propagate with characteristic lengths and celerities. The fluidized beds were filmed with a high-speed camera, and the images were processed by using numerical codes in order to automatically identify and track the formed patterns.*

Keywords: *bi-dispersed, fluidized bed, solid-liquid, narrow tubes, transverse waves.*

1. INTRODUCTION

A solid-liquid fluidized bed (SLFB) is a suspension of solid particles (grains) in a vertical tube submitted to an ascendant liquid fluid flow. Due to their high heat and mass transfer characteristics between solid particles and liquid medium, solid-liquid fluidized beds have been widely employed in chemical, environmental, and hydrometallurgical processes, especially in mineral processing industries where they are important to separate particles based on particle size, density, and shape (Nicolas *et al.*, 1999; Guazzelli, 2005; Zhang *et al.*, 2013; Tripathy *et al.*, 2013). The successful scale up, design and operation of solid-liquid fluidized beds mainly depend on the accurate prediction of the behavior and features of the system, such as phase holdups and their distributions, flow patterns, and mixing levels of the individual phases (Limtrakul *et al.*, 2005). Scientific fundamental research concerns the hydrodynamic structure of solid-liquid (patterns), and the equilibrium forces for fluid-particle and particle-particle interactions in fluidized beds. Taking into account the physical parameters of a liquid-solid system, the patterns formed by the solid particles in the bed is a function of superficial liquid velocity (Yang and Renken, 2003). Uniform fluidized beds are uncommon in industrial facilities, and usually instabilities appear. These instabilities consist of transverse waves, bubbles, or long bubbles.

Over the past decades, many papers investigated the flow regimes in solid-liquid fluidized beds (Nicolas *et al.*, 1999; Anderson and Jackson, 1968, 1969; El-Kaissy and Homsy, 1976; Didwania and Homsy, 1981; Zenit *et al.*, 1997; Zenit and Hunt, 2000; Duru and Guazzelli, 2002; Duru *et al.*, 2002; Aguilar-Corona *et al.*, 2011; Ghatage *et al.*, 2014). Some few papers investigated solid-liquid fluidized beds in narrow pipes (Anderson and Jackson, 1969; Zenit *et al.*, 1997; Zenit and Hunt, 2000; Duru *et al.*, 2002; Aguilar-Corona *et al.*, 2011; Ghatage *et al.*, 2014; Cúñez and Franklin, 2018b). Although there is not a consensus about it, we consider in this paper that for a narrow pipe the ratio between the tube and grain diameters is less than approximately 50. For solid-liquid fluidized beds in narrow tubes, the dynamics and instabilities are different due to high confinement effects; therefore, this case is still to be understood. Cúñez and Franklin (2018b,a) studied the behavior of liquid fluidized beds for a mono-dispersed distribution in a very narrow tube, using alumina beads with 6mm diameter, with a specific gravity of 3.69, and two water flow rates. With these conditions, high-compactness regions known as plugs were formed along the tube. The lengths of plugs were around $12d$ for $\overline{U}$ = 0.137 m/s and $7d$ for $\overline{U}$ = 0.164 m/s. The bed celerities in the upward direction varied between 0.012 and 0.060 m/s and in the downward direction between -0.019 and -0.114 m/s.

For bi-dispersed solid-liquid fluidized beds, the flow behavior of such beds is not well understood due to the lack of accurate experimental and numerical data. So, it is important to understand the bed expansion behavior, particle intermixing and/or segregation. These characteristics govern the flow patterns of solid and liquid phases thereby indirectly affecting the rates of mass and momentum transfer (Khan *et al.*, 2017; Jain *et al.*, 2017). Some studies have investigated the behavior of bi-dispersed fluidized beds over the last years (Epstein *et al.*, 1981; Gibilaro *et al.*, 1986; Escudié *et al.*,

2006; Di Maio and Di Renzo, 2016). Some of these authors studied the layer inversion phenomena and mixing that occurs by the presence of two different particles' distribution (size and density). However, no one studied the patterns formed by bi-dispersed solid-liquid fluidized beds in very narrow tubes.

In this paper we investigate the patterns appearing in a SLFB in very narrow tubes. Confinement effects caused by the narrow tube combined with the lubrication and virtual mass forces, which are significant under water, are the origin of alternating high- and low-compactness regions, known as plugs or clusters and bubbles, respectively. Although this instability is present in industrial applications, there have been very few studies about it, and its dynamics is still to be understood. Hence, the objective of this study is to obtain experimentally the lengths and celerities of granular plugs and granular clusters in very narrow tubes for a bi-dispersed case. The experimental results are presented for the first time in this paper.

2. EXPERIMENTAL SETUP

The schematic of the experimental device is presented in Fig.1. The experimental setup basically consisted of a water reservoir, a heat exchanger, a centrifugal pump, a flow meter, a flow homogenizer, a 25.4 mm-ID tube with vertical and horizontal sections, and a return line. Therefore, the water flowed in a closed loop in the order described above.

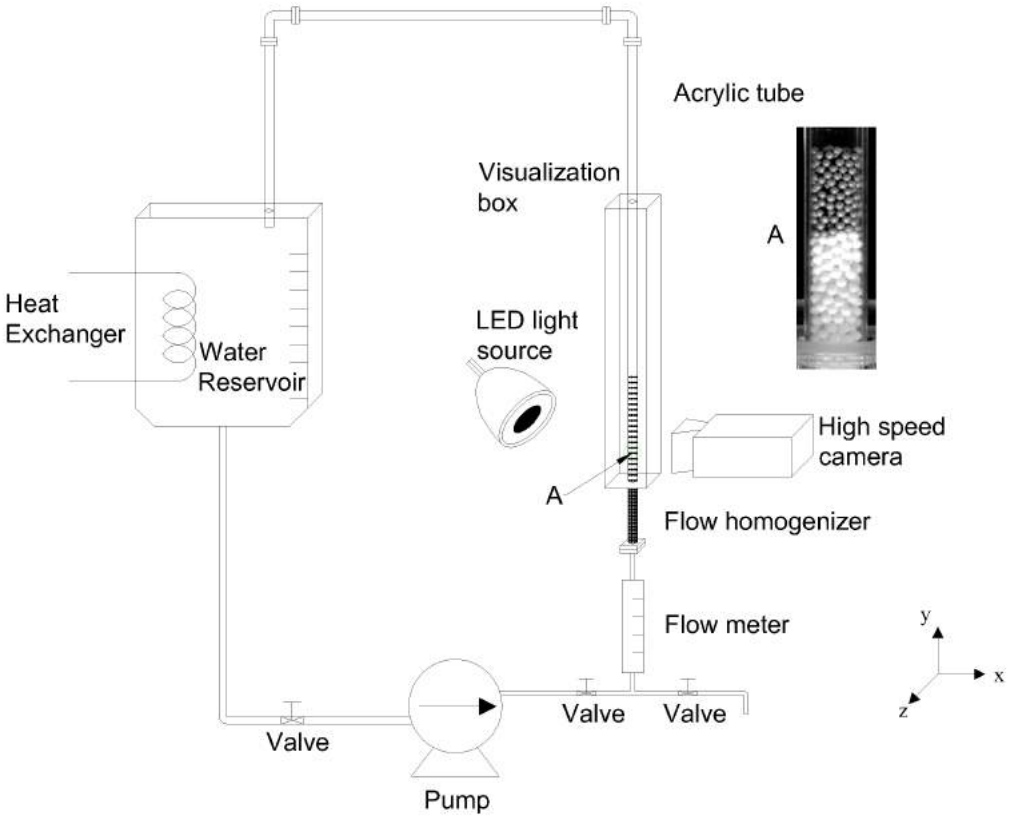

Figure 1. Layout of the experimental setup.

The vertical section was a 1.2 m-long, 25.4 mm-ID transparent PMMA (Polymethyl methacrylate) tube, of which 0.65 m was the test section. The vertical tube was vertically aligned within $\pm 3^{\circ}$. A visualization box filled with water was mounted in the test section to ensure proper photographic images. A flow homogenizer consisting of a fixed bed of packed alumina spheres with $d = 6$ mm was used to provide uniform water flows at the inlet of the test section. The water temperature was maintained at 24°C $\pm$ 3°C by a heat exchanger mounted in the water reservoir. The water flow rates were adjusted with a set of globe valves.

Alumina spheres (d_O =6$\pm$0.03 mm, $S_O = 3.69$) and aluminum spheres (d_A =4.762$\pm$0.1 mm, $S_A = 2.76$) were used as the solid phase, where d is the bead diameter and $S = \rho_p/\rho_f$ is the specific gravity. Six different arrangements of beds were used to develop the experiments. In order to better understand the arrangements, we designate the alumina beads by the subscript *O*, and the aluminum beads by the subscript *A*. The arrangements of beds were made by varying from 150 to 250 spheres of alumina and aluminum. We added the groups of particles by two ways into the tube. First, the aluminum

beads were inserted under the alumina beads, in this case the layer inversion phenomena occurred at the beginning of experiments, after that, both groups formed the patterns explained in the introduction. Finally, the alumina beads were inserted under the aluminum beads, forming only the patterns. Therefore, the arrangements used in this study are showed in Tab. 1.

Table 1. Arrangements of the beds used in the experiments.

$Arrangement$	$Code$	$N\,particles$ $Alumina$	$N\,particles$ $Aluminum$	$Order$
I	O150_A250	150	250	A under O
II	O250_A150	250	150	A under O
III	O250_A250	250	250	A under O
IV	A150_O250	250	150	O under A
V	A250_O150	150	250	O under A
VI	A250_O250	250	250	O under A

The Stokes and Reynolds numbers based on terminal velocities were $St_t = \overline{\rho_p} v_t \overline{d_p}/9\mu_f$ = 1062 and $Re_t = \rho_f v_t \overline{d_p}/\mu_f$ = 2980, respectively, where v_t is the terminal velocity of one single particle, μ_f is the dynamic viscosity of the fluid, $\overline{d_p}$ is the mean diameter and $\overline{\rho_p}$ is the mean solid density of the two particle species present in the bi-dispersed fluidized bed. The bed heights at the inception of fluidization h_{mf} for alumina beads were in average 64 and 102 mm, and for aluminum beads were in average 28 and 51 mm for the beds consisting of 150 and 250 particles, respectively, from which the liquid volume fraction at the inception of fluidization ε_{mf} was computed for each particle specie. The settling velocity at the inception of fluidization, computed based on the generalized Richardson–Zaki correlation for bi-dispersed fluidized beds, was $v_s = v_t \varepsilon_{mf}^{\overline{n}}$ = 0.09 m/s (Asif, 1998). Two water flow rates were imposed, Q = 250 l/h and Q = 300 l/h, for which the corresponding superficial velocities $\overline{U} = 4Q/\pi D^2$, fluid velocities trough the packed bed $U_f = \overline{U}/\varepsilon_{mf}$, Reynolds numbers based on the tube diameter $Re_D = \rho_f \overline{U} D/\mu_f$, and Reynolds numbers based on the grain diameter $Re_{\overline{d}} = \rho_f \overline{U d_p}/\mu_f$ are summarized in Tab. 2.

Table 2. Mean grain diameter $\overline{d_p}$, mean grain density $\overline{\rho_p}$, terminal Reynolds number Re_t, terminal Stokes number St_t, water flow rate Q, superficial velocity $\overline{U}$, Reynolds number based on the tube diameter Re_D, Reynolds number based on the mean diameter $Re_{\overline{d}}$, settling velocity v_s, and fluid velocities trough the packed bed U_f.

$\overline{d_p}$ mm	$\overline{\rho_p}$ kg/m^3	Re_t $\cdots$	St_t $\cdots$	Q l/h	$\overline{U}$ m/s	Re_D $\cdots$	$Re_{\overline{d}}$ $\cdots$	v_s m/s	U_f m/s
5.3	3209	2980	1062	250	0.137	3481	725	0.09	0.29
5.3	3209	2980	1062	300	0.164	4177	870	0.09	0.35

The solid-liquid fluidized beds were filmed with a high-speed camera of CMOS (Complementary Metal Oxide Semiconductor) type having a resolution of 1600 px × 2560 px at frequencies up to 1400 Hz at full resolution. To provide the necessary light for low exposure times while avoiding beating between the light source and the camera frequency, LED (Low Emission Diode) lamps were branched to a continuous current source. In this study, the camera frequency was set to between 100 Hz and 200 Hz. The number of acquired images for each test was 5000 and the total number of tests was 12, giving a total of 60000 images to be analyzed. MATLAB scripts were written in order to process the obtained images.

3. RESULTS

Under the tested conditions, high-compactness regions (plugs and clusters) and liquid bubbles (void regions) occupying the entire tube cross section were observed in the bi-dispersed fluidized bed. As explained in the previous section, a particular segregation state by density is reached after a certain period of time, i.e., alumina beads flow beneath aluminum beads for all experiments. So, it was possible to track the patterns formed by both alumina and aluminum beads. Those patterns, that were nearly one dimensional, propagated upwards with characteristic lengths and celerities.

Figures 2 and 3 present some frames obtained with the high-speed camera for the arrangements IV, V and VI for both flow rates, respectively. The corresponding times are in the caption of figures. From these figures, we can observe the plugs, clusters and bubbles in the bed.

The upward propagation of the void regions made the top of the bed and the interface between the alumina and aluminum particles oscillate between minimum and maximum values. Due to this oscillation, we computed the average height of the fluidized bed h_{avg} and the average height of the interface hi_{avg} as the average between minimum and maximum values. In addition, we computed the upward, C_{up}, Ci_{up}, and downward, C_{down}, Ci_{down}, celerities of the top

(a) (b) (c)

Figure 2. Instantaneous snapshots of particles positions: (a) Arrangement IV and $\overline{U}$ = 0.137 m/s; (b) Arrangement V and $\overline{U}$ = 0.137 m/s; (c) Arrangement VI and $\overline{U}$ = 0.137 m/s. The corresponding times are: (i) 0 s; (ii) 1 s; (iii) 2 s; (iv) 3 s; (v) 4 s; (vi) 5 s; (vii) 6 s.

(a) (b) (c)

Figure 3. Instantaneous snapshots of particles positions: (a) Arrangement IV and $\overline{U}$ = 0.164 m/s; (b) Arrangement V and $\overline{U}$ = 0.164 m/s; (c) Arrangement VI and $\overline{U}$ = 0.164 m/s. The corresponding times are: (i) 0 s; (ii) 1 s; (iii) 2 s; (iv) 3 s; (v) 4 s; (vi) 5 s; (vii) 6 s.

and the interface as the derivative of the measured positions during its rise and descent, respectively.

We identified and followed each granular plug and cluster in the high-speed movies by using numerical scripts. We present next the length scales and the celerities obtained from the experiments. Tables 3 and 4 present the arrangements of the beds, initial bed height h_{mf}, length scale of plugs normalized by the alumina diameter λ_p/d_O, standard deviation of length scale of plugs normalized by the alumina diameter $\sigma_{\lambda p}/d_O$, length scale of clusters normalized by the aluminum diameter λ_c/d_A, standard deviation of length scale of clusters normalized by the aluminum diameter $\sigma_{\lambda c}/d_A$, bed upward celerity C_{up}, standard deviation of bed upward celerities $\sigma_{C,up}$, bed downward celerity C_{down}, standard deviation of bed downward celerities $\sigma_{C,down}$, interface upward celerity Ci_{up}, standard deviation of interface upward celerities $\sigma_{Ci,up}$, interface downward celerity Ci_{down}, standard deviation of interface downward celerities $\sigma_{Ci,down}$, average height of the fluidized bed h_{avg}, and average height of the interface hi_{avg}, for each flow rate, respectively.

Within the experimental conditions, the lengths of plugs show strong variations with the water flow and are independent of the arrangement, despite the small variation in water superficial velocities (of only 20 %) when compared to the variation in the number of alumina particles (of 70 %). The lengths of plugs were around $7d$ for $\overline{U}$ = 0.137 m/s and $5d$ for $\overline{U}$ = 0.164 m/s. This represents a variation of 50 % in λ_p for variations of 20 % in $\overline{U}$. Standard deviations of plug lengths are large. On the other hand, the lengths of clusters show smooth variations with the water flow and are also independent of the arrangement. The lengths of clusters were around $3.4d$ for $\overline{U}$ = 0.137 m/s and $3.7d$ for $\overline{U}$ = 0.164 m/s. This represents a variation of 8 % in λ_c for variations of 20 % in $\overline{U}$. Standard deviations of cluster lengths are also large.

Table 3. Arrangement of the bed, initial bed height h_{mf}, length scale of plugs normalized by the alumina diameter λ_p/d_O, standard deviation of length scale of plugs normalized by the alumina diameter $\sigma_{\lambda p}/d_O$, length scale of clusters normalized by the aluminum diameter λ_c/d_A, standard deviation of length scale of clusters normalized by the aluminum diameter $\sigma_{\lambda c}/d_A$, bed upward celerity C_{up}, standard deviation of bed upward celerities $\sigma_{C,up}$, bed downward celerity C_{down}, standard deviation of bed downward celerities $\sigma_{C,down}$, interface upward celerity Ci_{up}, standard deviation of interface upward celerities $\sigma_{Ci,up}$, interface downward celerity Ci_{down}, standard deviation of interface downward celerities $\sigma_{Ci,down}$, average height of the fluidized bed h_{avg}, and average height of the interface hi_{avg}, for $\overline{U}$ = 0.137 m/s.

Arrangement	$\cdots$	I	II	III	IV	V	VI
h_{mf}	m	0.115	0.13	0.153	0.13	0.115	0.153
λ_p/d_O	$\cdots$	4.57	9.09	7.30	8.03	3.90	9.63
$\sigma_{\lambda p}/d_O$	$\cdots$	0.94	4.05	3.83	3.93	1.09	3.71
λ_c/d_A	$\cdots$	3.67	3.11	3.65	2.93	2.81	4.02
$\sigma_{\lambda c}/d_A$	$\cdots$	2.53	1.77	2.47	1.69	1.72	2.72
C_{up}	m/s	0.0251	0.0220	0.0295	0.0209	0.0280	0.0268
$\sigma_{C,up}$	m/s	0.0165	0.0133	0.0177	0.0128	0.0161	0.0143
C_{down}	m/s	-0.0314	-0.0267	-0.0356	-0.0259	-0.0334	-0.0321
$\sigma_{C,down}$	m/s	0.0247	0.0204	0.0325	0.0219	0.0346	0.0228
Ci_{up}	m/s	0.0124	0.0130	0.0173	0.0117	0.0106	0.0099
$\sigma_{Ci,up}$	m/s	0.0081	0.0083	0.0230	0.0072	0.0072	0.0064
Ci_{down}	m/s	-0.0192	-0.0213	-0.0287	-0.0286	-0.0158	-0.0178
$\sigma_{Ci,down}$	m/s	0.0174	0.0202	0.0344	0.0329	0.0159	0.0162
h_{avg}	m	0.158	0.175	0.211	0.173	0.151	0.202
hi_{avg}	m	0.072	0.122	0.127	0.121	0.070	0.118

Table 4. Arrangement of the bed, initial bed height h_{mf}, length scale of plugs normalized by the alumina diameter λ_p/d_O, standard deviation of length scale of plugs normalized by the alumina diameter $\sigma_{\lambda p}/d_O$, length scale of clusters normalized by the aluminum diameter λ_c/d_A, standard deviation of length scale of clusters normalized by the aluminum diameter $\sigma_{\lambda c}/d_A$, bed upward celerity C_{up}, standard deviation of bed upward celerities $\sigma_{C,up}$, bed downward celerity C_{down}, standard deviation of bed downward celerities $\sigma_{C,down}$, interface upward celerity Ci_{up}, standard deviation of interface upward celerities $\sigma_{Ci,up}$, interface downward celerity Ci_{down}, standard deviation of interface downward celerities $\sigma_{Ci,down}$, average height of the fluidized bed h_{avg}, and average height of the interface hi_{avg}, for $\overline{U}$ = 0.164 m/s.

Arrangement	$\cdots$	I	II	III	IV	V	VI
h_{mf}	m	0.115	0.13	0.153	0.13	0.115	0.153
λ_p/d_O	$\cdots$	3.73	5.62	4.53	6.24	3.73	4.94
$\sigma_{\lambda p}/d_O$	$\cdots$	1.87	3.28	2.59	3.71	1.81	2.71
λ_c/d_A	$\cdots$	4.04	3.12	3.01	5.13	3.06	3.94
$\sigma_{\lambda c}/d_A$	$\cdots$	2.99	1.93	2.09	3.03	2.13	3.07
C_{up}	m/s	0.0338	0.0335	0.0374	0.0329	0.0349	0.0325
$\sigma_{C,up}$	m/s	0.0231	0.0162	0.0246	0.0199	0.0212	0.0232
C_{down}	m/s	-0.0360	-0.0387	-0.0477	-0.0323	-0.0442	-0.0352
$\sigma_{C,down}$	m/s	0.0313	0.0298	0.0393	0.0239	0.0408	0.0330
Ci_{up}	m/s	0.0338	0.0342	0.0350	0.0298	0.0295	0.0339
$\sigma_{Ci,up}$	m/s	0.0162	0.0162	0.0192	0.0135	0.0144	0.0159
Ci_{down}	m/s	-0.0636	-0.0586	-0.0706	-0.0441	-0.0490	-0.0716
$\sigma_{Ci,down}$	m/s	0.0582	0.0570	0.0701	0.0403	0.0512	0.0653
h_{avg}	m	0.208	0.226	0.269	0.223	0.198	0.268
hi_{avg}	m	0.093	0.158	0.157	0.157	0.089	0.156

As seen in figures 2 and 3, the behavior of the bed and interface celerities is different for the aluminum and alumina beads, respectively. Bed celerities present variations with both the arrangement and flow conditions. For all the arrangements, C_{up} varies from 0.021 to 0.029 m/s for $\overline{U}$ = 0.137 m/s and from 0.033 to 0.037 m/s for $\overline{U}$ = 0.164 m/s, while C_{down} varies from -0.026 to -0.035 m/s for $\overline{U}$ = 0.137 m/s and from -0.033 to -0.047 m/s for $\overline{U}$ = 0.164 m/s. This represents variations of 35 % in C_{up} and C_{down} for any variation of the arrangements, and of 75 % in C_{up} and C_{down} for variations of 20 % in $\overline{U}$. For the case of interface, the celerities also present variations with both the arrangement and flow

conditions. For all the arrangements, Ci_{up} varies from 0.010 to 0.017 m/s for $\overline{U}$ = 0.137 m/s and from 0.030 to 0.035 m/s for $\overline{U}$ = 0.164 m/s, while Ci_{down} varies from -0.016 to -0.028 m/s for $\overline{U}$ = 0.137 m/s and from -0.045 to -0.070 m/s for $\overline{U}$ = 0.164 m/s. This represents variations of 35 % in C_{up} and 65 % in C_{down} for any variation of the arrangements, and of 250 % in Ci_{up} and 340 % in Ci_{down} for variations of 20 % in $\overline{U}$. These variations have the same order of magnitude of the variations presented in Cúñez and Franklin (2018a). As for λ_p/d_O and λ_c/d_A, standard deviations of the celerities are large.

In order to understand the distribution of the lengths of plugs and clusters along the tube, we computed the probability density functions (PDF) of the lengths of plugs normalized by the alumina diameter d_O, and of the lengths of clusters normalized by the aluminum diameter d_A, for both water flow rates. Figure 4 a) shows the probability density function of the lengths of the plugs normalized by the alumina diameter for each arrangement of beds and $\overline{U}$ = 0.137 m/s. From this figure, we can observe for the arrangement V, the distribution of the plugs lengths presents a different behavior when compared to the other five arrangements. For the arrangement I and V, the lengths of plugs are around 3 and 5d, respectively, with a little deviation, while for the other arrangements, the lengths of plugs are around 12d with a large deviation. This behavior is also observed in tables 3 and 4, when the values of λ_p/d_O and σ_{λ_p}/d_O are compared. Figure 4 b) shows the probability density function of the lengths of the plugs for the six arrangements of beds and $\overline{U}$ = 0.164 m/s. From this figure, we can observe the distribution of the plugs lengths presents the same behavior for all the arrangements, where the lengths of the plugs are around 4d. For the first flow rate, the superficial velocity $\overline{U}$ is slightly higher than the settling velocity v_s, i.e., the flow rate is closer to minimum fluidization; therefore, with a small amount of alumina spheres as the case of the arrangements I and V with N_O = 150, the formation of only two plugs is expected, as observed in Fig. 2 b), and this could be the explanation for the behavior of the Fig.4 a).

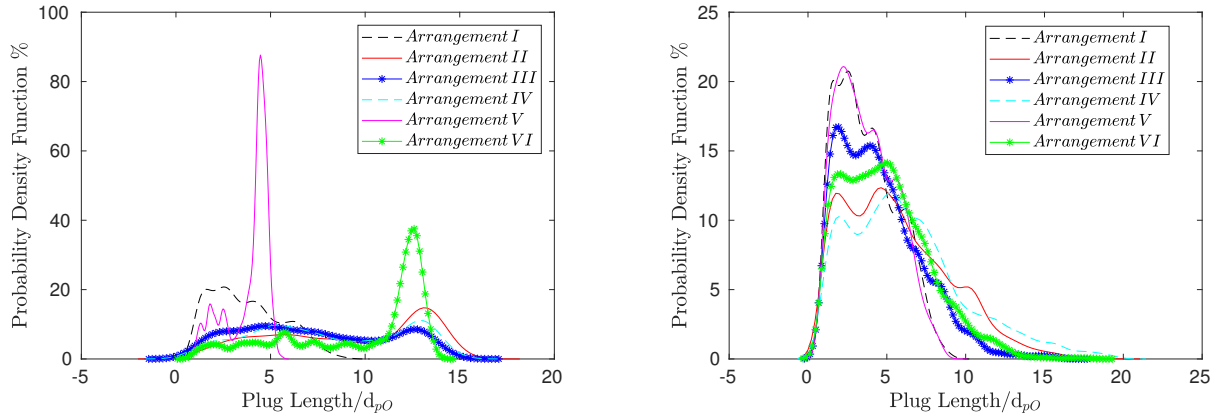

Figure 4. Probability density function of lengths of the alumina plugs for the six arrangements of beds: (a) $\overline{U}$ = 0.137 m/s; (b) $\overline{U}$ = 0.164 m/s.

Figure 5 a) shows the probability density function of the lengths of the clusters normalized by the aluminum diameter for each arrangement of beds and $\overline{U}$ = 0.137 m/s. From this figure, we can observe the distribution of the clusters lengths presents the same behavior for all the arrangements, where the lengths of the clusters are around 3d. Figure 5 b) shows the probability density function of the lengths of the clusters for the six arrangements of beds and $\overline{U}$ = 0.164 m/s. From this figure, we can also observe that the distribution of the clusters lengths presents the same behavior for all the arrangements, where the lengths of the clusters are around 3d. This behavior is also observed in tables 3 and 4, when the values of λ_c/d_A and σ_{λ_c}/d_A are compared. In the case of the clusters formed by the aluminum beads, it is possible to observe that these clusters are independent of variations in the flow rates and in the arrangements.

4. CONCLUSIONS

This paper investigated experimentally the patterns formed on bi-dispersed water fluidized beds in narrow tubes. The confinement created by the narrow tube together with the lubrication and virtual mass forces lead to the formation of alternating high- and low-compactness regions, known as plugs or clusters and bubbles, which have characteristic lengths and celerities. Although these patterns are presented in industrial applications, few previous studies were made to understand the problem, without exhausting it.

In the present study, fluidized beds were formed in a 25.4 mm-ID tube and consisted of alumina beads with 6 mm diameter and specific density of 3.69 and aluminum beads with 4.762 mm and a specific density of 2.76 fluidized by water flows. The ratio between the tube and the spheres was between 4.23 to 5.33, which was considered a very narrow case. In our experiments, the fluidized beds were filmed with a high-speed camera, and the plugs and clusters were automatically

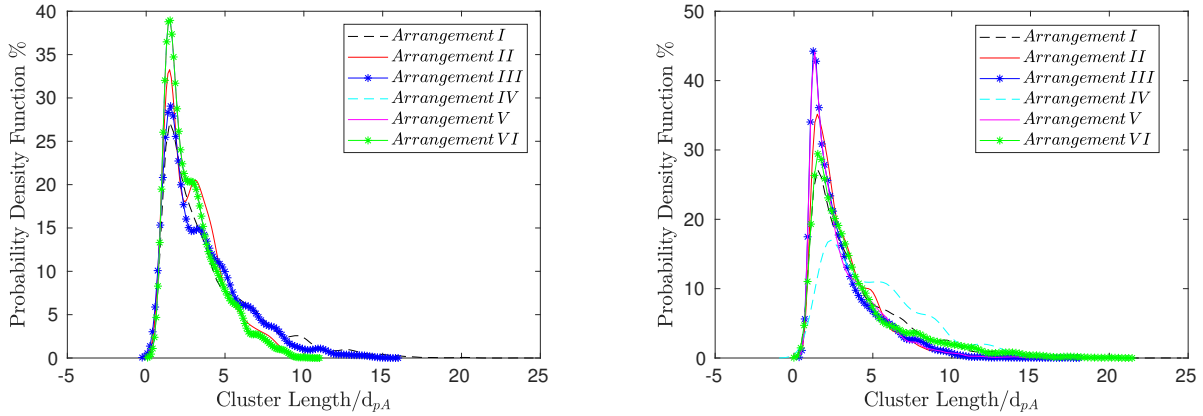

Figure 5. Probability density function of lengths of the aluminum clusters for the six arrangements of beds: (a) $\overline{U}$ = 0.137 m/s; (b) $\overline{U}$ = 0.164 m/s.

identified and tracked along images by using numerical scripts.

Under the experimental conditions, high compactness and void regions occupying the entire tube cross section were observed in the bi-dispersed fluidized bed. Despite the small variation in water superficial velocities when compared to the variation of the arrangements, the lengths of plugs strongly depended on the water flow and were independent of the arrangement of the bed. Unlike the lengths of clusters, that were independent for both the water flow and the arrangement of the bed. The behavior of the plugs was similar when compared with a mono-dispersed fluidized bed in a narrow tube (Cúñez and Franklin, 2018b,a).

From our experiments, we found that the lengths of plugs were around $7d$ for $\overline{U}$ = 0.137 m/s and $5d$ for $\overline{U}$ = 0.164 m/s, and the lengths of clusters were around $3d$ for both flow rates. The bed celerities in the upward direction varied between 0.021 and 0.037 m/s and in the downward direction between -0.033 and -0.047 m/s. Finally, the interface celerities in the upward direction varied between 0.010 and 0.035 m/s and in the downward direction between -0.016 and -0.070 m/s.

5. ACKNOWLEDGEMENTS

Fernando David Cúñez Benalcázar is grateful to FAPESP (grant no. 2016/18189-0), and Erick de Moraes Franklin would like to express his gratitude to FAPESP (grant no. 2016/13474-9) and CNPq (grant no. 400284/2016-2) for the financial support they provided.

6. REFERENCES

Aguilar-Corona, A., Zenit, R. and Masbernat, O., 2011. "Collisions in a liquid fluidized bed". *Int. J. Multiphase Flow*, Vol. 37, No. 7, pp. 695 – 705.

Anderson, T.B. and Jackson, R., 1968. "Fluid mechanical description of fluidized beds. Stability of the state of uniform fluidization". *Ind. Eng. Chem. Fundamen.*, Vol. 7, pp. 12–21.

Anderson, T.B. and Jackson, R., 1969. "A fluid mechanical description of fluidized beds. Comparison of theory and experiment". *Ind. Eng. Chem. Fundamen.*, Vol. 8, No. 1, pp. 137–144.

Asif, M., 1998. "Generalized richardson-zaki correlation for liquid fluidization of binary solids". *Chemical engineering & technology*, Vol. 21, No. 1, pp. 77–82.

Cúñez, F.D. and Franklin, E.M., 2018a. "Experimental investigation of liquid-solid fluidized beds in a narrow tube". In *Proceedings of the 17th Brazilian Congress of Thermal Sciences and Engineering - ENCIT 2018*. Aguas de Lindoia, SP, Brazil.

Cúñez, F.D. and Franklin, E.M., 2018b. "Plug regime in water fluidized beds in very narrow tubes". *Submitted, Powder Technology*.

Di Maio, F.P. and Di Renzo, A., 2016. "Direct modeling of voidage at layer inversion in binary liquid-fluidized bed". *Chemical Engineering Journal*, Vol. 284, pp. 668–678.

Didwania, A.K. and Homsy, G.M., 1981. "Flow regimes and flow transitions in liquid fluidized beds". *Int. J. Multiphase Flow*, Vol. 7, No. 6, pp. 563–580.

Duru, P. and Guazzelli, É., 2002. "Experimental investigation on the secondary instability of liquid-fluidized beds and the formation of bubbles". *J. Fluid Mech.*, Vol. 470, pp. 359–382.

Duru, P., Nicolas, M., Hinch, J. and Guazzelli, É., 2002. "Constitutive laws in liquid-fluidized beds". *J. Fluid Mech.*, Vol.

452, pp. 371–404.

El-Kaissy, M.M. and Homsy, G.M., 1976. "Instability waves and the origin of bubbles in fluidized beds: Part 1: Experiments". *Int. J. Multiphase Flow*, Vol. 2, No. 4, pp. 379 – 395.

Epstein, N., Leclair, B. and Pruden, B., 1981. "Liquid fluidization of binary particle mixtures-i: Overall bed expansion". *Chemical Engineering Science*, Vol. 36, No. 11, pp. 1803–1809.

Escudié, R., Epstein, N., Grace, J. and Bi, H., 2006. "Effect of particle shape on liquid-fluidized beds of binary (and ternary) solids mixtures: segregation vs. mixing". *Chemical Engineering Science*, Vol. 61, No. 5, pp. 1528–1539.

Ghatage, S.V., Peng, Z., Sathe, M.J., Doroodchi, E., Padhiyar, N., Moghtaderi, B., Joshi, J.B. and Evans, G.M., 2014. "Stability analysis in solid-liquid fluidized beds: Experimental and computational". *Chem. Eng. J.*, Vol. 256, pp. 169 – 186.

Gibilaro, L., Di Felice, R., Waldram, S. and Foscolo, P., 1986. "A predictive model for the equilibrium composition and inversion of binary-solid liquid fluidized beds". *Chemical engineering science*, Vol. 41, No. 2, pp. 379–387.

Guazzelli, É., 2005. *Fluidized beds: from waves to bubbles*, Wiley-VCH Verlag GmbH & Co. KGaA, chapter 9, pp. 211–232.

Jain, V., Kalo, L., Kumar, D., Pant, H.J. and Upadhyay, R.K., 2017. "Experimental and numerical investigation of liquid-solid binary fluidized beds: Radioactive particle tracking technique and dense discrete phase model simulations". *Particuology*, Vol. 33, pp. 112–122.

Khan, M.S., Mitra, S., Ghatage, S.V., Doroodchi, E., Joshi, J.B. and Evans, G.M., 2017. "Segregation and dispersion studies in binary solid-liquid fluidised beds: A theoretical and computational study". *Powder Technology*, Vol. 314, pp. 400–411.

Limtrakul, S., Chen, J., Ramachandran, P.A. and Duduković, M.P., 2005. "Solids motion and holdup profiles in liquid fluidized beds". *Chemical Engineering Science*, Vol. 60, No. 7, pp. 1889–1900.

Nicolas, M., Hinch, J. and Guazzelli, É., 1999. "Wavy instability in liquid-fluidized beds". *Ind. Eng. Chem. Res.*, Vol. 38, No. 3, pp. 799–802.

Tripathy, A., Sahu, A., Biswal, S. and Mishra, B., 2013. "A model for expansion ratio in liquid–solid fluidized beds". *Particuology*, Vol. 11, No. 6, pp. 789–792.

Yang, J. and Renken, A., 2003. "A generalized correlation for equilibrium of forces in liquid–solid fluidized beds". *Chemical Engineering Journal*, Vol. 92, No. 1-3, pp. 7–14.

Zenit, R. and Hunt, M.L., 2000. "Solid fraction fluctuations in solid-liquid flows". *Int. J. Multiphase Flow*, Vol. 26, No. 5, pp. 763 – 781.

Zenit, R., Hunt, M.L. and Brennen, C.E., 1997. "Collisional particle pressure measurements in solid-liquid flows". *J. Fluid Mech.*, Vol. 353, pp. 261–283.

Zhang, K., Guan, Y., Yao, X., Li, Y., Fan, X. and Brandani, S., 2013. "Two-and three-dimensional computational studies of liquid–solid fluidization". *Powder technology*, Vol. 235, pp. 180–191.

7. RESPONSIBILITY NOTICE

The following text, properly adapted to the number of authors, must be included in the last section of the paper:
The authors are the only responsible for the printed material included in this paper.